Eur. Phys. J. B **30**, 253–263 (2002)
DOI: 10.1140/epjb/e2002-00350-3

THE EUROPEAN PHYSICAL JOURNAL B

Dynamical scaling and kinetic roughening of single valued fronts propagating in fractal media

J. Asikainen[1,a], S. Majaniemi[1], M. Dubé[2], J. Heinonen[1], and T. Ala-Nissila[1,3]

[1] Helsinki Institute of Physics and Laboratory of Physics, Helsinki University of Technology, PO Box 1100, 02015 HUT, Espoo, Finland
[2] Department of Physics, 3600 University, McGill University, Montréal, QC, Canada H3A 2T8
[3] Department of Physics, Brown University, Providence, RI 02912–1843, USA

Received 22 May 2002
Published online 19 November 2002 –

Abstract. We consider the dynamical scaling and kinetic roughening of single-valued interfaces propagating in 2D fractal media. Assuming that the nearest-neighbor height difference distribution function of the fronts obeys Lévy statistics with a well-defined algebraic decay exponent, we consider the generalized scaling forms and derive analytic expressions for the local scaling exponents. We show that the kinetic roughening of the interfaces displays intrinsic anomalous scaling and multiscaling in the relevant correlation functions. We test the predictions of the scaling theory with a variety of well-known models which produce fractal growth structures. Results are in excellent agreement with theory. For some models, we find interesting crossover behavior related to large-scale structural instabilities of the growing aggregates.

PACS. 68.35.Ct Interface structure and roughness – 47.53.+n Fractals – 61.43.Hv Fractals; macroscopic aggregates (including diffusion-limited aggregates)

1 Introduction

Kinetic roughening of driven interfaces in random media is a ubiquitous phenomenon in nature. In addition to being a theoretically interesting and challenging problem in non-equilibrium statistical physics, kinetic roughening has important applications in *e.g.* crystal growth [1] and fluid invasion in porous media [2]. In many cases of interest, there is a description of kinetic roughening processes in terms of a stochastic equation of motion for the (single-valued) height function $h(\mathbf{x}, t)$. The best known example is the Kardar-Parisi-Zhang (KPZ) equation [3]

$$\frac{\partial h(\mathbf{x},t)}{\partial t} = \nu\nabla^2 h(\mathbf{x},t) + \frac{\lambda}{2}|h(\mathbf{x},t)|^2 + \eta, \qquad (1)$$

where η is a noise term. For strongly driven interfaces, the noise term is usually uncorrelated in space and time, but in some cases it may also depend on h in which case the noise is quenched. The KPZ equation and its variants with different types of noise have been analyzed extensively. Another interesting and more recent class of problems concerns cases where the equation of motion for $h(\mathbf{x}, t)$ is *non-local* due to *e.g.* an underlying conservation law in the system [4–6]. For such cases, it's not generally possible to write down a local equation of motion of the form of equation (1). However, both classes of growth equations typically lead to algebraic scaling of the relevant height correlation functions, with associated scaling exponents whose values are known exactly in some special cases.

There also exist interesting connections between kinetic roughening and more general theories of scale-invariant structures [1,7]. An important special case is the connection to percolation theory [8] for fronts which become pinned due to quenched disorder [2]. There are two particularly interesting universality classes arising from the quenched KPZ description near pinning, namely the isotropic percolation and directed percolation depinning (DPD) cases [9]. These two differ by their scaling exponents, as well as by the behavior of the nonlinear term in the underlying KPZ equation. Another case related to percolation is that of the propagation of interfaces in a background which itself undergoes a percolation transition and is thus a fractal [10,11]. This situation arises in phase-field models of slow combustion fronts [10], and "forest fire" lattice models [11]. The corresponding interfaces are forced to be single-valued by defining the height variable $h(\mathbf{x}, t)$ at each x to be the highest point where "burning" or "burned" trees appear. In this isotropic percolation depinning (IPD) case [11], some of the scaling exponents of the fronts can be directly related to the geometric properties of the underlying percolation cluster similar to the DPD case [9]. However, in the IPD limit there exists no KPZ

[a] e-mail: joo@fyslab.hut.fi

type of description for the interface dynamics. In addition to percolation, nontrivial fractal structures emerge from many growth models, including Diffusion Limited Aggregation [12] and various oblique-incidence ballistic growth models [1]. The current understanding of the roughening properties of fronts in such fractals is still rather incomplete.

In this work, our aim is to examine the problem of kinetic roughening of *single-valued* fronts in different types of fractal media. To this end, we study front propagation and kinetic roughening in three different classes of fractal models: the invasion percolation (IP) models [13], the diffusion limited aggregation (DLA) model [12], and the ballistic deposition (BD) model [14] with an uniform distribution of launch angles. We have recently shown both analytically and numerically [15], that for the IP models the results can be explained by the underlying Lévy statistics of the nearest-neighbor (NN) interface height differences. From such an algebraic distribution of the NN slopes we have derived exact expressions for some of the scaling exponents of fronts in the IP model. In the present work we present a more general and detailed derivation of the scaling exponents, and generalized scaling forms for the relevant correlation functions. In particular, we show that in addition to the local roughness exponents, the global roughness exponent χ is determined by the decay exponent of the NN slopes and is thus unambiguously related to the geometry of the fractal structure. We also show that the dynamical growth processes induce multiscaling [16] and anomalous intrinsic scaling [17] of the height difference correlation functions. We then proceed with numerical simulations of the three models described above. Results for the IP models are in excellent agreement with the analytic predictions. For the DLA and BD models, however, we find additional, more complex behavior. The decay exponents of the corresponding NN slope distribution functions depend on the system size, and the functions display non-algebraic tails for large enough slopes. This is related to the shadowing instability in the DLA and BD cases, and it can lead to the vanishing of multiscaling behavior in these models. Such crossover phenomena have been reported in ballistic growth models [18] and DLA type of models describing electrochemical deposition experiments [19].

2 Scaling properties of single-valued interfaces

For any interface propagating in a random medium, we define a set of single-valued local interface heights $\{h(x_i,t)\}_{i=1}^{L}$ at x_i by the highest occupied lattice site from the reference plane $h=0$ [11]. This corresponds to a solid-on-solid (SOS) description of the interface which excludes any overhangs belonging to the perimeter of a fractal cluster.

2.1 Classification of kinetic roughening

A rough surface may be characterized by the fluctuations of the height around its mean value. Thus, the basic quantity to look at is the *global* width

$$w_q(t,L) \equiv \langle \overline{[h(x,t)-\overline{h}(t)]^q} \rangle^{1/q}, \tag{2}$$

where the overbar denotes spatial averaging over x in a system of size L and angular brackets denote configuration (noise) averaging. For self-affine interfaces, the scaling of global widths is typically independent of q and satisfies the Family-Viscek (FV) scaling ansatz [20]

$$w(t,L) = t^{\beta} f(L/\xi(t)), \tag{3}$$

(where only the case $q=2$ is usually considered) with a scaling function $f(u)$ that satisfies

$$f(u) \sim \begin{cases} u^{\chi}, & \text{for } u \ll 1; \\ \text{const.}, & \text{for } u \gg 1. \end{cases} \tag{4}$$

In these equations χ is the roughness exponent and characterizes the stationary regime, in which the correlation length $\xi(t) \sim t^{1/z}$ has reached $\xi \approx L$. The quantity z defines the so-called dynamic exponent, and the ratio $\beta = \chi/z$ is called the growth exponent and characterizes the evolution of temporal correlations of the surface [2].

Some growth models exhibit different scaling of global and *local* interface fluctuations. This can be quantified by defining a local width of the interface $w(t,\ell)$ as

$$w(t,\ell) \equiv \langle \langle [h(x,t) - \langle h(t) \rangle_\ell]^2 \rangle_\ell \rangle^{1/2}, \tag{5}$$

where $\langle \cdots \rangle_\ell$ denotes an average over x in windows of spatial size ℓ. When local and global roughening processes differ, the surface is said to exhibit *anomalous scaling*. In this case, the scaling of the local width is of the form of equation (3), $w(t,\ell) \sim t^{\beta} f_A(\ell/\xi(t))$ with the anomalous scaling function $f_A(u)$ satisfying

$$f_A(u) \sim \begin{cases} u^{\chi_{\text{loc}}}, & \text{for } u \ll 1; \\ \text{const.}, & \text{for } u \gg 1, \end{cases} \tag{6}$$

where the new independent exponent χ_{loc} is called the local roughness exponent. Anomalous scaling has been found to occur in many growth models [21–23] as well as observed in experiments [24–26]. Anomalous scaling thus implies that there is one more independent exponent χ_{loc} describing local roughness of the interface. Experimentally, the local roughness exponent can be measured by direct methods since usually the system size is fixed. In fracture experiments [26] of systems with varying sizes both the local and global roughness exponents have been measured in good agreement with the scaling picture described above.

Recently, Ramasco *et al.* [17] proposed a generalized scaling theory. The corresponding scaling form incorporates all the different forms known thus far that dynamical scaling can take and predicts the existence of a new class

of growth models with novel anomalous scaling properties. Let $\hat{h}(k,t) = L^{-1/2}\sum_x [h(x,t) - \bar{h}(t)]\exp(\mathrm{i}kx)$ be the Fourier transform of the height of the surface in a system of size L. The whole scaling picture can be expressed in terms of the scaling of the structure factor

$$S(k,t) = \left\langle \hat{h}(k,t)\hat{h}(-k,t) \right\rangle . \tag{7}$$

Note that the other quantities such as the global and local width can be obtained from $S(k,t)$ [17]. If the roughening process under consideration shows generic dynamic scaling, that is $\xi(t) \sim t^{1/z}$ for small times and $\xi \sim L$ in the saturated regime [17], then the scaling of the structure factor is given by

$$S(k,t) = k^{-(2\chi+1)} s\left(kt^{1/z}\right), \tag{8}$$

where the scaling function has the general form

$$s(u) \sim \begin{cases} u^{2(\chi-\chi_s)}, & \text{for } u \gg 1; \\ u^{2\chi-1}, & \text{for } u \ll 1, \end{cases} \tag{9}$$

and the exponent χ_s is called the *spectral* roughness exponent. Now, the scaling properties of the interface can be classified according to the values of χ, χ_{loc}, and χ_s as follows [17]:

$$\begin{cases} \text{if } \chi_s < 1 \Rightarrow \chi_{\mathrm{loc}} = \chi_s \begin{cases} \chi_s = \chi \Rightarrow \text{Family} - \text{Vicsek}; \\ \chi_s \neq \chi \Rightarrow \text{Intrinsic anomalous}; \end{cases} \\ \text{if } \chi_s > 1 \Rightarrow \chi_{\mathrm{loc}} = 1 \quad \begin{cases} \chi_s = \chi \Rightarrow \text{Superrough}; \\ \chi_s \neq \chi \Rightarrow \text{New class}. \end{cases} \end{cases} \tag{10}$$

The difference between superroughening and intrinsic anomalous roughening has already been noted by López *et al.* [27]. All other classes can be distinguished from the difference between local and global scaling of the width, but the new scaling class is distinguishable from the structure factor only [17]. It will be shown in Section 3 that here the growing interfaces are intrinsically anomalous, and they exhibit *multiscaling* in terms of the local exponents.

2.2 Correlation functions

To quantitatively study the nature of the interface fluctuations we consider in addition to the structure factor a set of correlation functions. The behavior of the temporal and spatial correlation functions describing local properties of growing interfaces indicates whether or not anomalous scaling is present. Self-affine surfaces that obey the FV scaling have the same global and local roughness exponents. In the case of growing fractal aggregates studied here, global and local scaling differ.

To examine the spatiotemporal development of the interfaces, we define the qth order height difference correlation function as

$$G_q(x,t) = \langle \overline{|h(x_0,t) - h(x_0+x,t)|^q} \rangle^{1/q}, \tag{11}$$

with G_q satisfying the anomalous scaling relation [11,27]

$$G_q(x,t) = \xi^{\alpha_q} x^{\chi_q} f_q(x/\xi). \tag{12}$$

Here, the scaling function $f_q(u \to 0) = \text{const.}$ and $f_q(u \to \infty) \propto u^{-\chi_q}$ [11]. The exponents α_q define the so-called anomaly exponents, and χ_q's define local roughness exponents, with $\chi_{\mathrm{loc}} = \chi_2$ in equation (10).

A quantity measuring the temporal development of the local roughness of the interfaces is the average nearest neighbor height difference function $\sigma_q(t)$, defined by [21]

$$\sigma_q(t) = \langle \overline{|h(x_{i+1},t) - h(x_i,t)|^q} \rangle^{1/q}, \tag{13}$$

which at early times follows the scaling relation

$$\sigma_q \sim \xi^{\alpha_q} \sim t^{\alpha_q/z} \sim t^{\beta_q}, \tag{14}$$

where β_q's are the local growth exponents. At late times, σ_q's saturate to system size dependent values.

One can also define the time-dependent qth order height-height fluctuation correlation function

$$C_q(t_0,t) = \langle \overline{[\delta h(x,t_0) - \delta h(x,t_0+t)]^q} \rangle^{1/q}, \tag{15}$$

where $\delta h \equiv h - \overline{h}$ is the deviation from the average height. In the saturated regime, one expects C_q to scale as $C_q \sim t^{\tilde{\beta} q}$ at early times, and to saturate to a system size dependent value at large times.

3 Exact results for scaling exponents

3.1 Local slope distributions

For the case of the KPZ equation without quenched randomness, it is well known [2] that the steady-state distribution of (coarse-grained) local slopes of the height variables ∇h in 1D is Gaussian, $P(\nabla h) \sim \exp[-(\nabla h)^2]$. This leads to a self-affine interface whose height difference profile is equivalent to the trajectory of a 1D random walk, and thus $\chi = 1/2$ characterizing the "width" of the walk. However, in systems where quenched noise is present, the underlying probability distributions are typically of Lévy type, that is, they have an algebraic decay form [7]. In our previous work [15], we have shown that this is indeed the case for the IP models. Here, we present the arguments in more detail.

Let us consider the case where the distribution function $P(\Delta h)$ for local nearest-neighbor (NN) slopes $\Delta h \equiv |h(x_{i+1}) - h(x_i)|$ has a Lévy distribution of the form

$$P(\Delta h) \sim (\Delta h)^{-\alpha}, \tag{16}$$

where $\alpha > 1$ [7,15]. Equation (16) can be used to derive expressions for the local scaling exponents in the following way. Let $|\Delta h|_{\max}$ denote the largest of the NN slopes. We can assume that

$$[\sigma_q(t)]^q \approx \int_0^{|\Delta h|_{\max}} \mathrm{d}(\Delta h) P(\Delta h) (\Delta h)^q. \tag{17}$$

For the maximum height differences, asymptotically $|\Delta h|_{\max} \sim w_\infty(t) \sim t^\beta$, since by equation (2), w_∞ measures only the largest of the height differences and there is no q dependence in the scaling of the global width. Thus, we obtain

$$\sigma_q(t) \sim t^{[1+(1-\alpha)/q]\beta}, \tag{18}$$

which means that the local growth exponents are given by

$$\beta_q = \left(1 + \frac{1-\alpha}{q}\right)\beta. \tag{19}$$

The local roughness exponent can be obtained by combining the scaling of $\sigma_q(t)$ and $G_q(x,t)$ (Eqs. (12) and (14) with $x \approx \xi \approx L$). Using $\chi_q + \alpha_q = \chi$ and the fact that $\beta_q z = \alpha_q$, and requiring that α is independent of q, we find that

$$\chi_q = 1/q. \tag{20}$$

The requirement that a unique, well-defined α exists yields a prediction for the *global* roughness exponent as

$$\chi = \frac{1}{\alpha - 1}\,. \tag{21}$$

These arguments show that both the local and global roughness exponents are uniquely determined by the statistics of the NN slopes which is the fundamental quantity here. Moreover, the local χ_q's are "superuniversal" in the sense that they don't depend on the algebraic exponent α. Our results also show that multiscaling [16] and intrinsic anomalous roughening occur for $\alpha > 1$, but that the interfaces are never superrough since $\chi_{\rm loc} = \chi_2 = 1/2$. The present arguments, however, give no information about β (or z) which describes the true *dynamics* of the interfaces. Also, to obtain the β_q's as given in equation (19), the global β needs to be determined. Its value depends on the details of the dynamical rules of interface propagation even if the statistical properties of the underlying quenched noise are the same [11,15].

Similar values for the local roughness exponent $\chi_{\rm loc}$ were recently observed for roughening of fluid front in Hele-Shaw cell [28]. In these experiments, the columnar nature of the quenched disorder also induces large slopes in the interface. Further, the local slope distribution was shown to have a power-law decay form [29].

Recently, López [30] has introduced a scaling approach to calculate scaling exponents from actual continuum equations describing surface growth. By considering the scaling of the mean square local derivative (or slope) of the interface height, $s(t) = \langle\overline{(\nabla h)^2}\rangle \sim t^{2\kappa}$, he has shown that the interfaces exhibits anomalous scaling whenever the scaling exponent $\kappa > 0$. This exponent corresponds exactly to our $\beta_2 = [1+(1-\alpha)/2]\beta$, which is here positive for $1 < \alpha < 3$. However, in the present case everything is determined by the NN slope distribution, and no assumptions are needed about the possible existence of a (local) growth equation or the form of a coarse-grained slope distribution function.

3.2 Generalized scaling

To explain the scaling behavior of $C_q(t_0,t)$ we define a generalized correlation function $\tilde{C}_q(x,t_0,t)$ as

$$\tilde{C}_q(x,t_0,t) \equiv \langle\overline{|\delta h(x_0,t_0) - \delta h(x_0+x,t_0+t)|^q}\rangle^{1/q}. \tag{22}$$

By definition, it has the following limits:

$$\begin{cases} \tilde{C}_q(x,t_0,0) = G_q(x,t_0); \\ \tilde{C}_q(1,t_0,0) = \sigma_q(t_0); \\ \tilde{C}_q(0,t_0,t) = C_q(t_0,t). \end{cases} \tag{23}$$

Next we define two dimensionless scaling variables as $u_1 \equiv x/\xi(t_0)$ and $u_2 \equiv t/t_0$. In terms of these we propose the following scaling form for $\tilde{C}_q$:

$$\tilde{C}_q(x,t_0,t) = \xi(t_0)^{\alpha_q} x^{\chi_q} \tilde{f}_q(u_1,u_2). \tag{24}$$

First, for $u_2 = 0$, we must obtain the scaling form of $G_q(x,t_0)$. Therefore, $\tilde{f}_q(u_1,0) = f_q(u_1) \propto u_1^{-\chi_q}$ for $u_1 \gg 1$. For small times t_0 this gives $G_q(x,t_0) \propto t_0^{(\alpha_q+\chi_q)/z} \propto t_0^\beta$. Next, we consider a non-zero u_2. Taking the limit $x \to 0$ of $\tilde{C}_q$ we should recover C_q. Since the x dependence of $\tilde{C}_q$ must vanish, we require that $\tilde{f}_q(u_1,u_2) \propto u_1^{-\chi_q} g_q(u_2)$ for $u_1 \to 0$, where g_q is a new scaling function. Hence,

$$\begin{aligned} \lim_{x\to 0} \tilde{C}_q(x,t_0,t) &\to \xi(t_0)^{\alpha_q} x^{\chi_q} u_1^{-\chi_q} g_q(u_2) \\ &\propto t_0^\beta\, g_q(t/t_0) \propto C_q(t_0,t), \end{aligned} \tag{25}$$

where $g_q(u_2) \propto u_2^{\tilde{\beta}_q}$ for $u_2 \ll 1$. At this point, $\tilde{\beta}_q$ is unknown. In the opposite limit $u_2 \gg 1$ we expect that $g_q(u_2) = \text{const}$. This is an explicit scaling *prediction* for C_q. Next, we consider the known scaling limits of $\tilde{C}_q$ for $x = 1$ and for $x = 0$. We assume that the scaling behavior in t_0 of $\tilde{C}_q$ stays the same irrespective of whether we approach the origin $u_1 = u_2 = 0$ along the axis u_1 or u_2. Let us first set $u_2 = 0$ ($t = 0$):

$$\tilde{C}_q(x,t_0,0) = \xi(t_0)^{\alpha_q} x^{\chi_q} f_q(u_1). \tag{26}$$

Approaching the origin along the u_1 axis means that we set $x = 1$ (to make contact with σ_q) and require that $\xi(t_0)$ is so large that $u_1 = 1/\xi(t_0) \ll 1$. This yields the known scaling of σ_q:

$$\tilde{C}_q(1,t_0,0) \propto \xi(t_0)^{\alpha_q} \sim t_0^{\beta_q} \sim \sigma_q(t_0), \tag{27}$$

where we used the fact that $\beta_q = \alpha_q/z$. Next, we set $u_1 = 0$ ($x = 0$) with the result that $\tilde{C}_q$ reduces to C_q. Approaching the origin by setting $u_2 \ll 1$ we have

$$\tilde{C}_q(0,t_0,t) \sim t_0^\beta\, g_q(u_2) \sim t_0^\beta\, (t/t_0)^{\tilde{\beta}_q} \sim t^{\tilde{\beta}_q}\, t_0^{\beta-\tilde{\beta}_q}. \tag{28}$$

The two limits given by equations (27, 28) are different in the sense that the latter goes to zero when $t \to 0$, whereas

the former stays finite for all values of t_0 (no matter how small $u_1 = 1/\xi(t_0)$ becomes; only if we set $x = \epsilon$ and let $\epsilon \to 0$ will $\tilde{C}_q(\epsilon, t_0, 0)$ go to zero as well). However, taking the scaling in variable t_0 to be the same in both limiting cases, we are able to derive the final result for $\tilde{\beta}_q$:

$$\tilde{\beta}_q = \beta - \beta_q. \tag{29}$$

Scaling forms will be numerically tested in Section 5.3.

3.3 Finite size scaling

We can generalize the scaling of $\tilde{C}_q$ even further by postulating the following form:

$$\tilde{C}_q(x, t_0, t, L) = \xi(t_0)^{\alpha_q} x^{\chi_q} \tilde{f}_q(u_1, u_2, u_3), \tag{30}$$

where we have introduced a third dimensionless scaling variable $u_3 \equiv \xi(t_0)/L$, which was assumed to be zero in the previous section. It should be noted that equation (30) is exactly of the same form as what the scaling functions of linear growth theories would have [31]. Let us study the finite size scaling of C_q. Based on equation (25) we can write

$$C_q(t_0, t, L) \sim t_0^{\beta}\, g_q(u_2, u_3). \tag{31}$$

For a finite system, the correlation function should become independent of the origin of time t_0 in the saturated region. Therefore, for $t_0 \gg L^z$ ($u_3 \gg 1$) we assume that $g_q(u_2, u_3) \sim u_3^{\gamma_1} g'_q(u_2)$, where g'_q is a new scaling function and γ_1 some unknown scaling exponent. Because there is still some t_0 dependence left in the argument u_2 of g'_q we further assume that in the limit we are considering $g'_q(u_2) \sim u_2^{\gamma_2}$, where yet another unknown scaling exponent γ_2 has been introduced. Since all variables of C_q follow a power law scaling form, it is easy to get a condition for the vanishing of the t_0 dependence. For $u_3 \to \infty$, we have

$$C_q(t_0, t, L) \sim t_0^{\beta}\, u_3^{\gamma_1}\, g'_q(u_2) \sim t_0^{\beta}\, u_3^{\gamma_1}\, u_2^{\gamma_2} \tag{32}$$

$$\sim t_0^{\beta+\gamma_1/z-\gamma_2}\, t^{\gamma_2}\, L^{-\gamma_1}. \tag{33}$$

To get rid of t_0 we must set $\beta + \gamma_1/z - \gamma_2 = 0$. On the other hand we know that $C_q \sim t^{\tilde{\beta}_q}$ which fixes $\gamma_2 = \tilde{\beta}_q$. Knowing γ_2 it is easy to solve for γ_1:

$$\gamma_1 = z(\gamma_2 - \beta) = -z\beta_q. \tag{34}$$

Therefore, in the limit of large u_3 we can construct the finite size scaling form of C_q based on equation (33) as follows:

$$C_q(t, L) \sim L^{-\gamma_1} t^{\gamma_2} = L^{z\beta_q} t^{\tilde{\beta}_q} \tag{35}$$

$$= L^{z\beta_q} (t/L^z)^{\tilde{\beta}_q} L^{z\tilde{\beta}_q} = L^{\chi} (t/L^z)^{\tilde{\beta}_q}. \tag{36}$$

Thus, we predict that $C_q(t, L) = L^{\chi} F_q(t/L^z)$, where the new scaling function $F_q(s) \sim s^{\tilde{\beta}_q}$ for $s \ll 1$, in analogy with the FV scaling form.

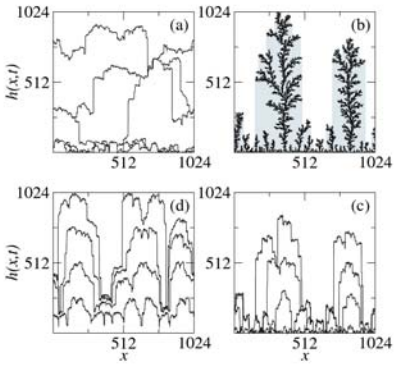

Fig. 1. (a) Snapshots of a series of single-valued interfaces as generated by the NTIP model. (b) Snapshot of a configuration generated by the DLA model. Grey shading shows how the overhangs are cut off to define the single-valued height profile. (c) Snapshots of a series of single-valued interfaces as generated by the DLA model. (d) Snapshots of a series of single-valued interfaces as generated by the BD model.

4 Fractal models

To study the validity of our theory of Section 3, we examine three well-known models involving interface dynamics in random media, namely the invasion percolation (IP) model [8], diffusion limited aggregation (DLA) [12], and a ballistic deposition model with uniform launch angle distribution (BD) [14]. These models are reviewed in this section, together with a short summary of the technical details of our numerical simulations.

4.1 Invasion percolation

Invasion percolation (IP) models [13] constitute an important and widely studied class of percolation theory. The IP is a dynamic percolation process that describes the displacement of one fluid by another in a porous medium in the limit where capillary forces dominate the viscous forces [8]. Figure 1a shows a sequence of single-valued interfaces generated by the model. IP can be divided in two cases: one with trapping (TIP) and the other without it (NTIP). TIP describes a situation in which the defender fluid is incompressible, and thus invasion process terminates in regions fully surrounded by invading fluid. The NTIP model, on the other hand, is consistent with the case where the defending fluid is compressible. An important property of the NTIP model is that it is believed to be equivalent to ordinary percolation [32] which means that its geometric properties are well known. The temporal development of IP clusters has been studied in references [33,34], and self-organization and kinetic roughening with local slope constraints in reference [35].

Here we study the IP model with periodic boundary conditions in the horizontal x direction and free boundaries in the vertical y direction. The numerical simulations

of the IP lattice models were done on a 2D square lattices of sizes $L \times L_y$, with $L = 32 - 4096$ and $L_y = L - 4L$. The bottom row is initially occupied by the invading fluid. At each time step, one searches for the nearest neighbor (NN) perimeter sites that are occupied by the defending fluid, chooses the one with the smallest capillary number and occupies it by the invading fluid. This process is then repeated until the invasion cluster reaches the top of the lattice. The main algorithmic aspect in our simulations is that the list of active growth sites is implemented via a balanced binary search tree (see *e.g.* Refs. [36–38]). By this method, the insertion and deletion operations on the list can be performed in time $\propto \ln(n)$, where n is the list size. In the case of TIP, one has to at each time step check if an the newly invaded site caused a region of defending fluid to be trapped [39]. If this is the case, the active perimeter sites within the trapped region are removed from the list of growth sites [40].

4.2 Diffusion limited aggregation

Diffusion limited aggregation (DLA) is a model of irreversible growth to generate fractal structures as proposed by Witten and Sander [12]. It has been used to study a great variety of processes: dendritic growth, viscous fingers in fluids, dielectric breakdown, electrochemical deposition etc. [41]. In spite of the apparent simplicity of the model, analytic solutions for most of its properties are still unavailable. A typical DLA cluster is shown in Figure 1b, with single-valued interfaces in c. As in the case of IP, we grow DLA clusters in cylindrical geometry, starting with an initially occupied bottom row. At each step, a walker is launched at a randomly chosen position on a line which is one lattice unit higher than the highest occupied site in the cluster. The walker then performs random walk until it sticks to the cluster. This process is then repeated until the desired cluster size is reached. To speed up the simulations, we use special techniques [42] that allow the walker to reach the already existing cluster faster. The largest lateral system size used in our DLA simulations was $L = 4096$.

4.3 Ballistic deposition

Ballistic deposition (BD) was introduced as a model of colloidal aggregates, and early studies concentrated on the properties of the porous aggregate produced by the model (see Ref. [2] and references therein). In the model, particles are deposited vertically at random positions. Particle follows a straight trajectory until it reaches the surface, where it sticks. We study a modified version of the original model, introduced by Karunasiri *et al.* [14], in which the launch angle is chosen from a distribution $P(\theta)$, with $-\pi < \theta < \pi$. In particular, we consider here the case with a uniform distribution for θ. Deposition with a distribution $P(\theta)$ with respect to the substrate normal leads to an instability, known as the shadow instability [14]. The shadow instability is due to the fact that parts of the surface which "stick out" may shadow nearby points thus retarding their growth. In the case of low-temperature sputter deposition of amorphous and polycrystalline thin films, the shadow instability is known to play a significant role in determining the surface morphology [43]. A series of single-valued interfaces generated by the BD model is shown in Figure 1d.

To enable simulations of large enough systems, we use bit-packing procedure for the BD model. Each 32 bit integer of the simulation lattice describes the state of 32 sites of the "macro-lattice". In practice, we pack the lattice in the direction perpendicular to the substrate. Thus the periodic boundaries in the parallel direction are easily implemented. The largest system size used in the BD simulations was $L = 131072$.

5 Results

In this section, we present our numerical results from computer simulations of the three models as described in the previous section. We will first demonstrate, that for all the three models considered here a Lévy type of slope distribution function follows, and then discuss direct numerical findings of the scaling exponents.

However, before this we note that it's possible to devise a simple test by simply generating interfaces directly from the Lévy distribution of equation (16). Such a model, of course, has no dynamics but the local roughness exponents can be easily determined from the spatial correlation functions. We have generated height profiles where independent NN height differences were drawn from the distribution $P(\Delta h) \sim \Delta h^{-\alpha}$ with $1 < \alpha < 3$. Our numerical estimates for the χ_q's support the prediction of equation (20), namely that they do not depend on the decay exponent α.

5.1 Local slope distributions and roughness exponents

According to our theoretical arguments, the fundamental quantity here is the NN height difference distribution function $P(\Delta h)$. We have determined this from direct numerical simulations of each model for single-valued interfaces in the late-time saturated regime. We have also determined both the global exponents using $w(L,t), S(k,t)$ and $G_q(x,t)$ and the local quantities from the appropriate correlation functions.

1. *Invasion percolation.* For the case of an isotropic percolation cluster, we have previously shown through an analytic argument that the exponent α is given exactly by $\alpha = (-\tau + 1)D = 2$, where $\tau = 187/91$ and $D = 91/48$ are the cluster size probability exponent and the cluster's fractal dimension, respectively [15]. From equation (21) this leads to the prediction that $\chi = 1$, which is also expected due to the spatial isotropy of the cluster [11]. In Figure 2 we show $P(\Delta h)$ as determined numerically for the NITP

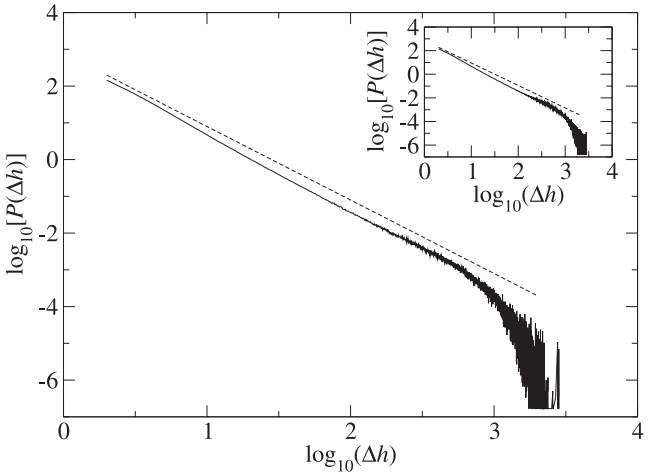

Fig. 2. The distribution function $P(\Delta h)$ for the NTIP model. Inset shows $P(\Delta h)$ for the TIP model. Dashed lines show the slope $\alpha = 2$. The system size for both cases is 1024.

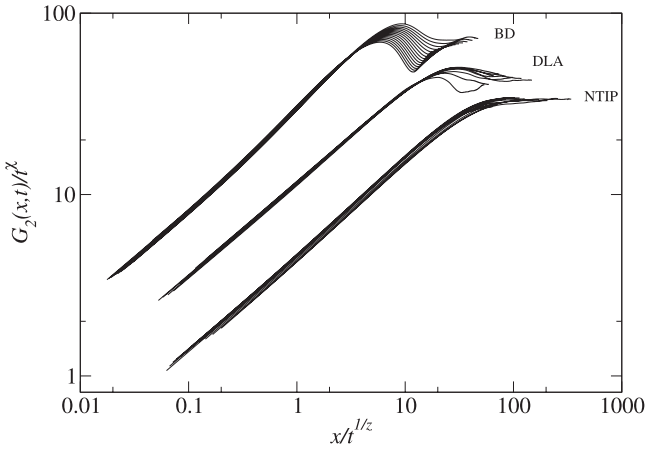

Fig. 3. Scaling of the correlation functions $G_2(x,t)$ for the three models. The groups of curves for different models have been shifted for clarity. The exponents used in the data collapse are $\chi = 1, 1.3,$ and 1.25, and $z = 1, 1,$ and 1.25 for the NTIP, DLA, and BD models, respectively.

Table 1. The local scaling exponents from numerical simulations of the NTIP model. Analytic predictions are shown in the lower part of the table.

q	β_q	$\tilde{\beta}_q$	χ_q
1	$\mathcal{O}(\log)$	0.95 ± 0.04	0.86 ± 0.01
2	0.51 ± 0.05	0.51 ± 0.01	0.51 ± 0.02
3	0.67 ± 0.04	0.33 ± 0.02	0.34 ± 0.02
4	0.73 ± 0.02	0.24 ± 0.01	0.26 ± 0.01
5	0.75 ± 0.03	0.19 ± 0.02	0.20 ± 0.02
6	0.77 ± 0.02	0.16 ± 0.02	0.17 ± 0.02
	$1 - 1/q$	$1/q$	$1/q$

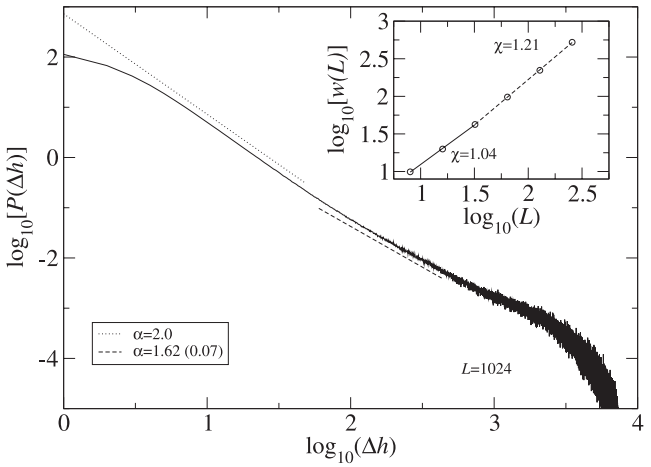

Fig. 4. The distribution function $P(\Delta h)$ for the DLA model for $L = 1024$. Inset shows the scaling of $w(L)$ with the system size L, with a clear crossover around $L = 16$. See text for details.

model, and we indeed find that $\alpha = 2.00 \pm 0.05$. For the global roughness exponent we find using equation (4) that $\chi = 0.99 \pm 0.02$. The local scaling exponents are found by computing the correlation functions of equation (11), and the results are in excellent agreement with the prediction $\chi_q = 1/q$. The scaling exponents are summarized in Table 1. We also verified the anomalous scaling form of equation (12) as shown in Figure 3.

In the inset of Figure 2 we also show results for the TIP model, for which $\alpha = 1.9 \pm 0.1$. Thus, within our numerical accuracy the two models have the same α, and thus identical roughness exponents. This is not a trivial result since numerical estimates for the TIP model give $D \approx 1.82$ [13], a value somewhat lower than $91/48 \approx 1.90$.

2. *Diffusion Limited Aggregation.* For the DLA case the distribution function is given in Figure 4, for a system of size $L = 1024$. An interesting feature in $P(\Delta h)$ is that there seem to be roughly three regimes in it. For $10 \lesssim \Delta h \lesssim 50$, the effective α has a value of close to 2.0, after which it levels off to about $\alpha = 1.6 \pm 0.1$. According to our predictions changing α should change χ, and we have verified this by directly computing χ from the global width for systems of different sizes. The results are in the inset of Figure 4. Two distinct scaling regimes are visible, with $\chi = 1.05 \pm 0.03$ and $\chi = 1.21 \pm 0.04$ for the set of smaller and larger system sizes, respectively. We also measured the global roughness exponent from $S(k,t)$ to be $\chi = 1.35 \pm 0.10$, in agreement with the second regime. Again, the local χ_q's are in excellent agreement with theory, as can be seen in Table 2. Finally, for $\Delta h \gtrsim 1000$ there is a distinct bump in $P(\Delta h)$. At the end of this section we will argue that for large enough values of Δh, the distribution has a non-algebraic form, leading to further observable changes in the scaling behavior.

Table 2. The local scaling exponents from numerical simulations of the DLA model. The determination of the growth exponents is discussed in the text. Analytical predictions are shown in the lower part of the table, and they agree with simulations for $\alpha \approx 2$, $\beta = 1.35$.

q	β_q	$\tilde{\beta}_q$	χ_q
1	0.27 ± 0.03	0.89 ± 0.04	0.86 ± 0.03
2	0.71 ± 0.03	0.49 ± 0.03	0.52 ± 0.02
3	0.91 ± 0.02	0.32 ± 0.02	0.36 ± 0.02
4	1.01 ± 0.02	0.24 ± 0.02	0.27 ± 0.02
5	1.07 ± 0.02	0.19 ± 0.02	0.22 ± 0.02
6	1.11 ± 0.02	0.15 ± 0.02	0.19 ± 0.02
	$[1 + (1 - \alpha)/q]\beta$	$\beta - \beta_q$	$1/q$

Table 3. The local scaling exponents from numerical simulations of the BD model. Determination of the growth exponents is discussed in the text. Analytic predictions are shown in the lower part of the table, and they agree with simulations for $\alpha \approx 2.1$, $\beta = 1.16$.

q	β_q	$\tilde{\beta}_q$	χ_q
1	0.0 ± 0.1	0.86 ± 0.04	0.97 ± 0.03
2	0.51 ± 0.03	0.50 ± 0.03	0.54 ± 0.03
3	0.66 ± 0.03	0.32 ± 0.02	0.37 ± 0.03
4	0.73 ± 0.02	0.24 ± 0.02	0.28 ± 0.02
5	0.78 ± 0.02	0.19 ± 0.02	0.23 ± 0.02
6	0.81 ± 0.02	0.15 ± 0.02	0.19 ± 0.02
	$[1 + (1 - \alpha)/q]\beta$	$\beta - \beta_q$	$1/q$

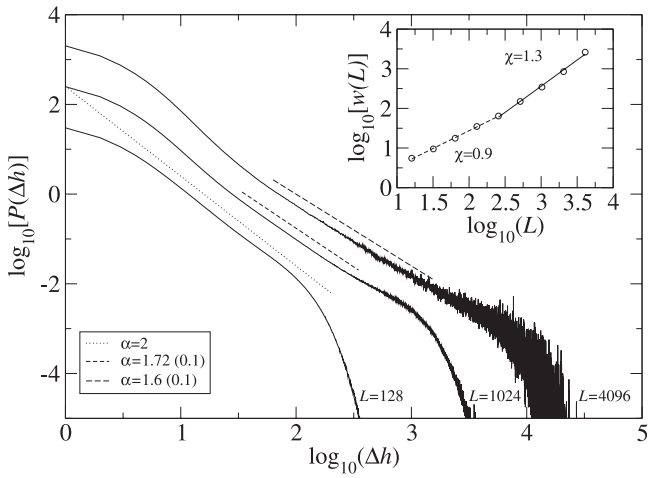

Fig. 5. A series of distribution functions $P(\Delta h)$ for the BD model for different system sizes. Changes in the effective slopes are evident (see text for details). Inset shows the scaling of $w(L)$ with the system size L, with a crossover around $L = 128$.

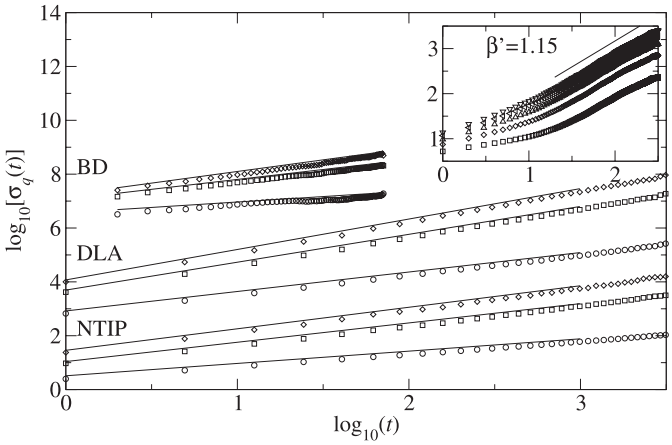

Fig. 6. Correlation functions $\sigma_q(t)$ for $q = 2, 4,$ and 6 (from bottom to top) for the models studied. For the BD case, we plot $\log[\sigma_q(2t) - \sigma_q(t)]$ here. Solid lines indicate the fits (see Tabs. 1, 2 and 3). Fitted curves have been shifted for clarity. Inset: $\sigma_q(t)$ for the BD model as in the main figure. After the first crossover time curves turn parallel, and multiscaling in time vanishes (see text for details). From bottom to top, data are for $q = 2, 3, \ldots, 6$.

3. *Ballistic Deposition.* Conclusions similar to that of the DLA case apply to the BD model as well. In Figure 5 we show three slope distribution functions, for systems of sizes $L = 128$, 1024, and 4096. In these three cases, the different regimes are clearly visible. For the smallest system, α is very close to 2.0, while for the larger systems the effective values of α for larger slopes are reduced to about 1.7 ± 0.1 and 1.6 ± 0.1, respectively. The inset shows χ as measured directly from the global width, showing how the effective χ tends to increase with system size corresponding to the decreasing slope distribution exponent. Again, a bump is visible in $P(\Delta h)$ for the largest slopes. In reference [44] $\chi \approx 1$ was measured for the BD model, corresponding to smaller system sizes as in the inset. The local roughness exponents are summarized in Table 3.

5.2 Temporal scaling and correlation functions

1. *Invasion percolation.* We have measured β directly from $w(t)$ and find that it grows linearly in time, *i.e.* $\beta = 1.00 \pm 0.03$. This indicates that the dynamic exponent $z = 0.99 \pm 0.05$. This differs from the so-called isotropic percolation depinning [11] case for which $z = d_{\min}$, where $d_{\min} \approx 1.13$ is the minimum distance exponent of the underlying isotropic 2D percolation cluster. In particular, this demonstrates how changing the dynamical rules from those of the NTIP model to the nearest-neighbor "forest fire" model of reference [11] changes the growth exponent. Regarding local scaling, the temporal qth order correlation functions defined in equation (13) were evaluated in the growth regime, and those of equation (15) in the saturated regime. Agreement with the theory is very good,

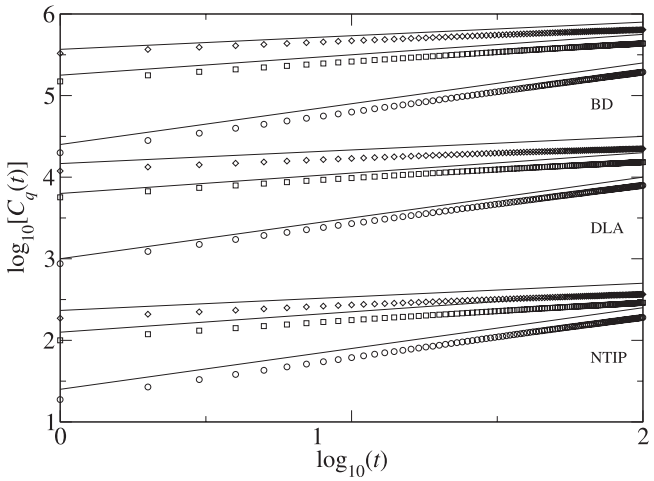

Fig. 7. Correlation functions $C_q(t)$ for $q = 2, 4,$ and 6 (from bottom to top) for the models studied. Solid lines indicate the fits (see Tabs. 1, 2 and 3). Fitted curves have been shifted for clarity.

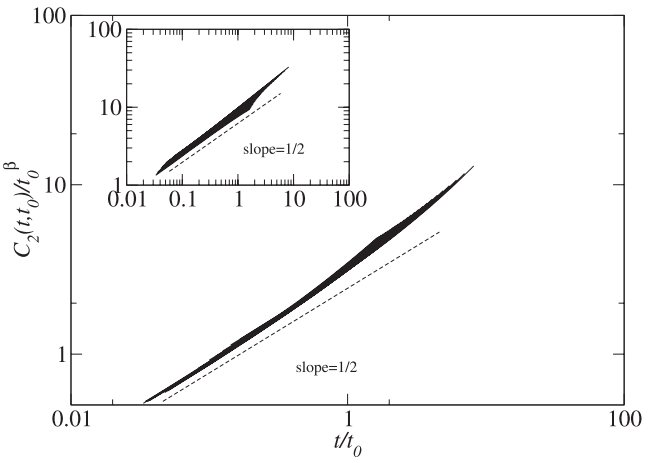

Fig. 8. The scaling function $g_2(t/t_0)$ of equation (25) for the BD model. The data are extracted from simulation with $L = 4096$. Inset shows the same function for the NTIP model. Here system size is $L = 2048$.

as can be seen in Figures 6 and 7, and Table 1. We note that for the NTIP case, equation (29) predicts that $\tilde{\beta}_q = 1/q$. The exponents β_q and $\tilde{\beta}_q$ were evaluated for the growing TIP interfaces as well. The numerical estimates are indistinguishable from the NTIP case.

2. *Diffusion Limited Aggregation.* The growth exponent is $\beta = 1.35 \pm 0.02$ as measured directly from $w(t)$ for $L = 4096$, and the dynamic exponent $z = 1.0 \pm 0.1$. The temporal qth order correlation functions defined in equation (13) were evaluated in the growth regime for $L = 4096$, and those of equation (15) in the saturated regime for $L = 2048$. Since the corresponding local exponents β_q and $\tilde{\beta}_q$ depend explicitly on α which itself changes with system size (and the magnitude of the NN slopes), it is not possible to pin down unique values for these exponents. Despite this problem, relatively good fits can be obtained for both temporal correlation functions as can be seen in Figures 6 and 7. In Table 2 we summarize the exponents from these fits. The values of β_q and $\tilde{\beta}_q$ are in good agreement with theory, when $\alpha \approx 2$ corresponding to the NN slope distribution of Figure 4 for smaller slope values.
3. *Ballistic Deposition.* Our estimate for the growth exponent is $\beta = 1.16 \pm 0.03$, as measured for the largest system of size $L = 131072$ from the global width $w(t)$. For smaller system sizes we measured a somewhat smaller value for the growth exponent $\beta \approx 0.95$. The estimate for the dynamic exponent is $z = 1.12 \pm 0.07$. The values measured in reference [44] differ slightly from our estimates. Regarding the local exponents β_q and $\tilde{\beta}_q$, in analogy to the DLA case it's not possible to pin them down uniquely. Data using systems of sizes $L = 65536$ for $\sigma_q(t)$, and $L = 2048$ for $C_q(t)$ are shown in Figures 6 and 7, respectively. The results of least-squares fitting are in Table 3. Again, when we use $\alpha \approx 2.1$ the numerical results are in good agreement with theory.

Above, we mentioned that the function $P(\Delta h)$ has a non-algebraic tail when NN slopes become large. This can in fact be seen from the NN height difference correlation function $\sigma_q(t)$. The functions $\sigma_q(t)$ for small t, have the q dependent power law exponents β_q as given by equation (19). However, for longer times these functions turn parallel as demonstrated in the inset of Figure 6 for the BD model with $L = 4096$. In this regime, the local growth exponents become independent of q. After another crossover time, the usual saturation regime begins. This means that the scaling of σ_q is given by

$$\sigma_q(t) \sim \begin{cases} t^{\beta_q}, & \text{for } t \ll L^z; \\ t^{\beta'}, & \text{for } t \approx L^z; \\ L^z, & \text{for } t \gg L^z, \end{cases} \tag{37}$$

where we find within our numerical accuracy that $\beta' \approx \beta$. Thus, multiscaling vanishes in this regime. Similar behavior has recently been seen in other DLA type of models describing electrochemical deposition experiments [19]. We think that this change is related to the well-known shadowing instability for the DLA and BD models [14], which leads into a change in the evolution of the interface morphology at later times. The effect of the shadow instability is also visible as a bump in the correlation functions $G_q(x,t)$ at large values of x corresponding to the spatial distance between the large "leaves" in the aggregates (see Fig. 3), or in the small k values of the structure factor. This conclusion is also supported by the fact that in the IP models, this phenomenon does not occur.

5.3 Scaling

To check the validity of the scaling formulas derived in Section 3.2, we have numerically evaluated the corresponding scaling functions. In Figure 8, the scaling function $g_2(t_0/t)$

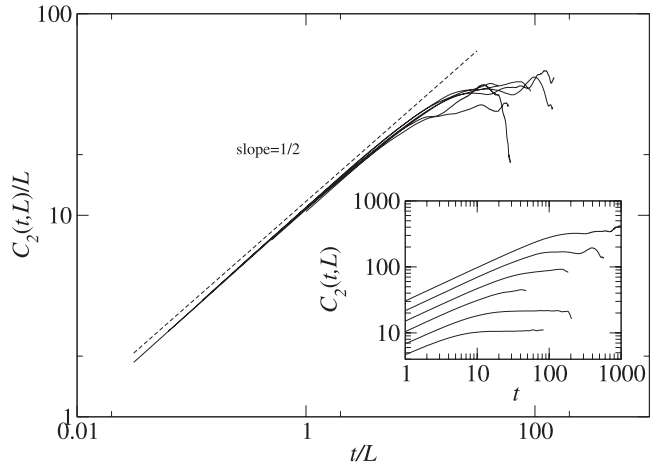

Fig. 9. Scaling of the correlation function $C_2(t, L)$ with the system size for the NTIP model. The range of system sizes is $L = 128, \ldots, 2048$, and inset shows the unscaled data. The correlation functions were evaluated in the saturated regime.

of equation (25) is shown for both the BD and NTIP models. These scaling functions show very strong finite size effects due to large fluctuations especially for higher moments q, so that large enough lattices must be used in the calculations.

Finally, the finite-size scaling for the functions $C_2(t, L)$ with various system sizes L is shown in Figure 9 for the NTIP model. The inset shows the raw data, and in the main figure we observe very good scaling as predicted by equation (36).

6 Conclusions

In this work, we have examined the dynamical scaling and kinetic roughening of driven single-valued fronts in 2D fractal media. First, through analytic arguments we have shown that the local NN slope distribution function obeys an algebraic decay law, with a decay exponent α which for isotropic percolation can be obtained from the known geometric exponents of the underlying fractal cluster. Based on the algebraic Lévy behavior, we have then considered generalized scaling of the relevant correlation functions, and derived exact expressions for the roughening exponents. Our results show that kinetic roughening under these circumstances is of intrinsic anomalous type, with multiscaling and explicitly q dependent local roughness exponents. Particularly remarkable is also the result that the global roughness exponent χ is completely and uniquely determined by the decay exponent α. This means that by measuring the scaling of single-valued fronts, one can obtain direct geometrical information about the underlying fractal cluster.

We have tested the theoretical predictions numerically by simulations of three well-known models which produce different spatial fractals. For the invasion percolation models, we find behavior in excellent agreement with theory. For the two other growth models, there is more complicated behavior due to the large-scale instabilities of the growing aggregate structures. Similar crossover behavior has also been observed in DLA type of models describing electrochemical deposition [19]. It would be of great interest to test these predictions experimentally.

Generous computer resources of the Center of Scientific Computing, Finland are acknowledged. We wish to thank M. Alava, M. Castro, R. Cuerno, and I. Koponen for useful discussions. This work has been supported in part by the Academy of Finland through its Center of Excellence program. J.A. wishes to thank the Vaisala Foundation for financial support.

References

1. J. Krug, Advances in Physics **46**, 139 (1997)
2. A.-L. Barabási, H.E. Stanley, *Fractal Concepts in Surface Growth* (Cambridge University Press, Cambridge, 1995)
3. M. Kardar, G. Parisi, Y.-C. Zhang, Phys. Rev. Lett. **79**, 889 (1986)
4. T. Salditt, H. Spohn, Phys. Rev. E **47**, 3524 (1993);
5. J. Heinonen, I. Bukharev, T. Ala-Nissila, J.M. Kosterlitz, Phys. Rev. E **57**, 6851 (1998)
6. M. Dubé, M. Rost, K.R. Elder, M. Alava, S. Majaniemi, T. Ala-Nissila, Phys. Rev. Lett. **83**, 1628 (1999); Eur. Phys. J. B **15**, 701 (2000)
7. M. Paczuski, S. Maslov, P. Bak, Phys. Rev. E **53**, 414 (1996); G. Huber, M.H. Jensen, K. Sneppen, Phys. Rev. E **52**, R2133 (1995)
8. D. Stauffer, A. Aharony, *Introduction to Percolation Theory*, revised 2nd edn. (Taylor and Francis, Burgess Science Press, Basingstoke, London, 1994)
9. L.-H. Tang, M. Kardar, D. Dhar, Phys. Rev. Lett. **74**, 920 (1995)
10. N. Provatas, T. Ala-Nissila, M. Grant, K.R. Elder, L. Piché, Phys. Rev. E **51**, 4232 (1995); J. Stat. Phys. **81**, 737 (1995)
11. M.P. Kuittu, M. Haataja, N. Provatas, T. Ala-Nissila, Phys. Rev. E **58**, 1514 (1998); *ibid.* **59**, 3774 (1999)
12. T.A. Witten, L.M. Sander, Phys. Rev. Lett. **47**, 1400 (1981)
13. D. Wilkinson, J. Willemsen, J. Phys. A **16**, 3365 (1983)
14. R.P.U. Karunasiri, R. Bruinsma, J. Rudnick, Phys. Rev. Lett. **62**, 788 (1989); G.S. Bales, A. Zangwill, Phys. Rev. Lett. **63**, 692 (1989)
15. J. Asikainen, M. Dubé, S. Majaniemi, T. Ala-Nissilä, Phys. Rev. E **65**, 052104 (2002)
16. A.-L. Barabási, R. Bourbonnais, M. Jensen, J. Kertész, T. Vicsek, Y.-C. Zhang, Phys. Rev. A **45**, R6951 (1992)
17. J.J. Ramasco, J.M. López, M.A. Rodríguez, Phys. Rev. Lett. 84, 2199 (2000)
18. J. Yao, C. Roland, H. Guo, Phys. Rev. A **45**, 3903 (1992)
19. M. Castro, R. Cuerno, A. Sánchez, F. Domínguez-Adame, Phys. Rev. E **57**, R2491 (1998)
20. F. Family, T. Viscek, J. Phys. A **18** L75 (1985)
21. J. Krug, Phys. Rev. Lett. **72**, 2907 (1994)
22. S. Das Sarma, C.J. Lanczycki, R. Kotlyar, S.V. Ghaisas, Phys. Rev. E **53** 359 (1996)
23. J.M. López, M.A. Rodríguez, Phys. Rev. E **54**, R2189 (1996)

24. H.-N. Yang, G.-C. Wang, T.-M. Lu, Phys. Rev. Lett. **73**, 2348 (1994)
25. J.H. Jeffries, J.-K. Zuo, M.M. Craig, Phys. Rev. Lett. **76**, 4931 (1996)
26. J.M. López, J. Schmittbuhl, Phys. Rev. E **57**, 6405 (1998)
27. J.M. López, M.A. Rodríguez, R. Cuerno, Phys. Rev. E, **56**, 3993 (1997)
28. J. Soriano, J.J. Ramasco, M.A. Rodríguez, A. Hernández-Machado, J. Ortín, Phys. Rev. Lett. **89**, 026102 (2002)
29. J. Soriano, J. Ortín, A. Hernández-Machado, `cond-mat/0208432` (2002)
30. J.M. López, Phys. Rev. Lett. **83**, 4594 (1999)
31. S. Majaniemi, T. Ala-Nissila, J. Krug, Phys. Rev. B **53**, 8071 (1996)
32. M. Dias, D. Wilkinson, J. Phys. A **19**, 3131 (1986)
33. S. Roux, E. Guyon, J. Phys. A, **22**, 3693 (1989)
34. L. Furuberg, J. Feder, A. Aharony, T. Jossang, Phys. Rev. Lett. **61**, 2117 (1988)
35. K. Sneppen, Phys. Rev. Lett. **69**, 3539 (1992), K. Sneppen, M.H. Jensen, Phys. Rev. Lett. **71**, 101 (1993)
36. S. Schwarzer, A. Shlomo, A. Bunde, Phys. Rev. E **59**, 3262 (1999)
37. A.P. Sheppard, M.A. Knackstedt, W.V. Pinczewski, M. Sahimi, J. Phys. A **32**, L521 (1999)
38. M.A. Knackstedt, M. Sahimi, A.P. Sheppard, Phys. Rev. E **61**, 4920 (2000)
39. All local configurations consisting of the newly invaded site and its eight neighbors are enumerated. The configurations that cause trapping are labelled, and at each time step one can by computing the configuration number decide whether trapping occurred or not
40. P. Meakin, Physica A **173**, 305 (1991)
41. T. Vicsek, *Fractal Growth Phenomena* (World Scientific, Singapore, 1992); For a review, see *Fractals in Natural Science*, edited by T. Vicsek, M. Schlesinger, M. Matsuhita (World Scientific, Singapore, 1993)
42. J. Asikainen, J. Heinonen, T. Ala-Nissilä, accepted in Phys. Rev. E
43. R.A. Roy, R. Messier, Mat. Res. Soc. Symp. Proc. **38**, 363 (1985); R. Messier, J.E. Yehoda, J. Appl. Phys. **58**, 3739 (1985); R. Messier, J. Vac. Sci. Technol. A **4**, 490 (1986); T. Salditt *et al.*, Europhys. Lett. **36**, 565 (1996)
44. J. Yu, J.G. Amar, Phys. Rev. E **66**, 021603 (2002)